Popular Summary

Persistent Nature of Secondary Diurnal Modes of Precipitation over Oceanic and Continental Regimes

Song Yang, Kwo-Sen Kuo, and Eric A. Smith

The first joint Tropical Rainfall Measuring Mission (TRMM) by the US National Aeronautics and Space Administration (NASA) and the Japan Aerospace Exploration Agency (JAXA) launched on November 22, 1997 provides unique long-term precipitation measurements over the global tropics. This study develops a powerful clock-face type graphic display method to clearly and accurately show the global patterns of the rainfall diurnal phase and amplitude at the same time, using the 8-year TRMM rainfall datasets. The late evening – early morning diurnal phase over ocean and mid-late afternoon diurnal phase over land are graphically displayed consistent with the global continents. This paper is also the first to show the globally spatial patterns of the minor diurnal phase and intensity of rainfall diurnal cycles. The impact of horizontally spatial scales on rainfall diurnal cycle is discussed. Results show that any selected spatial scale has no impact on the major diurnal peak of rainfall, but a significant impact on the minor diurnal peak. The advantages and disadvantages of using a harmonic analysis method in studying the rainfall diurnal cycle are discussed in detail. This method can exhibit global spatial patterns of the major diurnal peak, while suppressing the influence of rain noise on diurnal cycles. However, it reveals a weaker diurnal intensity and shifted phases. The possible false distribution of the minor diurnal peak caused by this method is physically and graphically explained.

Persistent Nature of Secondary Diurnal Modes of Precipitation over Oceanic and Continental Regimes

Song Yang[1], Kwo-Sen Kuo[2], and Eric A. Smith[3]

[1] Center for Earth Observing and Space Research, College of Science, George Mason University, Fairfax, VA; MailStop -- NASA/GSFC, Laboratory for Atmospheres (Code 613.1), Greenbelt, MD 20771, USA [301-614-6338 ; ysong@agnes.gsfc.nasa.gov]

[2] GEST/Caelum; MailStop -- NASA/GSFC, Laboratory for Atmospheres (Code 613.1), Greenbelt, MD 20771, USA [301-614-6277 ; kskuo@radar.gsfc.nasa.gov]

[3] NASA/Goddard Space Flight Center, Laboratory for Atmospheres (Code 613.1), Greenbelt, MD 20771, USA [301-614-6286 ; eric.a.smith@nasa.gov]

June 2007

For submission to a Special Issue in
Journal of Climate
"*Understanding Diurnal Variability of Precipitation through Observations and Models*"

Corresponding Author

Dr. Song Yang, Laboratory for Atmospheres (Code 613.1)
NASA/Goddard Space Flight Center
Greenbelt, MD, 20771 USA
Tel: (301) 614-6338; Fax: (301) 614-5492; Email: ysong@agnes.gsfc.nasa.gov

Abstract

This investigation seeks a better understanding of the assorted mechanisms controlling the global distribution of precipitation diurnal variability based on the use of Tropical Rainfall Measuring Mission (TRMM) microwave radiometer and radar data. The horizontal distributions of precipitation's diurnal cycle are derived from eight years of TRMM Microwave Imager (TMI) and Precipitation Radar (PR) measurements involving three TRMM standard rain rate retrieval algorithms -- the resultant distributions analyzed at various spatiotemporal scales. The results reveal the prominent and expected late-evening to early-morning (LE-EM) precipitation maxima over oceans and the counterpart prominent and expected mid- to late-afternoon (MLA) maxima over continents. Moreover, and not generally recognized, the results reveal a widespread distribution of secondary maxima occurring over both oceans and continents -- maxima which generally mirror their counterpart regime's behavior. That is, many ocean regions exhibit clear-cut secondary MLA precipitation maxima while many continental regions exhibit just as evident secondary LE-EM maxima. This investigation is the first comprehensive study of these globally prevalent secondary maxima and their widespread nature, a type of study only made possible when the analysis procedure is applied to a high-quality global-scale precipitation dataset.

The characteristics of the secondary maxima are mapped and described on global grids using an innovative clock-face format, while a current study to be published at a later date provides physically-based explanations of the seasonal-regional distributions of the secondary maxima. In addition to an "explicit" maxima identification scheme, a "Fourier decomposition" maxima identification scheme is used to examine the amplitude and phase properties of the primary and secondary maxima -- as well as tertiary and quaternary maxima. Accordingly, the advantages, ambiguities, and pitfalls resulting from use of Fourier harmonic analysis are explained.

1. Introduction

Studies of atmospheric diurnal processes which are influenced by the regulated daily cycle of incoming solar radiation at the top-of-atmosphere (TOA) have been taking place for over one hundred years. The seminal study of Hann (1901) was the first to address precipitation's diurnal cycle. Observational and modeling analyses have demonstrated that diurnal processes are evident in many atmospheric quantities. These include precipitation (e.g., Hong et al. 2005 and Yang and Smith 2006), surface temperature (e.g., Smith 1986), surface winds (e.g., Deser and Smith 1998), surface pressure (e.g., Petenko and Argentini 2002), vertical motion (e.g., Krishnamurti and Kishtawal 2000), cloudiness (e.g., Wylie and Woolf 2002), and surface (e.g., Smith et al. 1986) and TOA (e.g., Smith and Rutan 2003) radiation fluxes -- as foremost variables. Notably, lengthy time series derived from satellite measurements of various atmospheric variables have motivated new types of research concerning diurnal variability.

This has been particularly true for precipitation since the advent of Tropical Rainfall Measuring Mission (TRMM) and its associated TRMM Microwave Imager (TMI) radiometer and Precipitation Radar (PR) rain rate retrievals dating back to November 1997. Many mechanisms have been proposed to explain precipitation diurnal behavior. The "static radiation-convection" (SRC) mechanism (e.g., Randall et al. 1991), "dynamic radiation-convection" (DRC) mechanism (e.g., Gray and Jacobson 1977), "nighttime radiative cooling driven elevated relative humidity" (NRC-ERH) mechanism (e.g., Tao et al. 1996; Sui et al. 1997, 1998), or the slowly evolving, diurnally-varying "large scale vertical motion" (LS-VM) mechanism (e.g., McBride and Gray 1980) represent various possible explanations for the well-established "late evening-early morning" (LE-EM) oceanic surface precipitation maximum, while the diurnally-regulated surface solar radiative heating (SRH) mechanism, which can manifest itself in either

the form of a "static destabilization" (SD) mechanism or a "differential heating" (DH) mechanism, are the foremost explanations for the often-observed "mid- to late-afternoon" (MLA) continental surface precipitation maximum (e.g., Ramage 1971 and Pielke 2002). A number of studies using regional observations (e.g., Schwartz and Bosart 1979; Oki and Musiake 1994; Anderson et al 1996; Sui et al 1998; Chen et al. 1999; and Dai 2001) have reported a secondary LE-EM peak in the continental precipitation diurnal cycle. The main possible explanations for this mode, which have been reviewed by Yang and Smith (2006), consist of the "mobile terrain-forced precipitating system" (MTFPS) mechanism and a continentally-based NRC-ERH mechanism. There is also a counterpart MLA secondary peak in the oceanic precipitation diurnal cycle (e.g., McGarry and Reed 1978; Reed and Jaffe 1981; Augustine 1984; Fu et al. 1990; Serra and McPhaden 2004), for which the only plausible explanation that can be put forward is an ocean surface heating (OSH) mechanism, which can involve the near surface water layer (for oceans, seas, and inland lakes) and/or the moist boundary layer over the water.

However, there is yet to be and investigation of the secondary diurnal mode of precipitation as a global phenomenon. Yang and Smith (2006) provide a detailed review and analysis of the variety of mechanisms controlling the diurnal cycle of precipitation. Based on the use of TRMM precipitation data, their analysis demonstrated that precipitation diurnal variability is a global phenomenon with embedded diurnal forcing factors -- far more complex than can be explained with a few general causes (i.e., the approach followed by nearly all past literature concerning this topic). The primary and dominant LE-EM oceanic precipitation maximum is often accompanied by a secondary MLA maximum, while the primary and dominant MLA continental precipitation maximum is often accompanied or even replaced by a secondary LE-EM maximum.

As Yang and Smith (2006) emphasize, there are a host of mechanisms at work that produce the precipitation diurnal process, not one of which solely explains the entire process. Instead, a mixture of mechanisms whose individual components control regional and smaller scale diurnal modes work together to produce the averaged global process. Notably, most modeling studies investigating diurnal variability, particularly studies based on the atmospheric general circulation model (GCM), have focused on stand-alone monolithic mechanisms (e.g., Randall et al. 1991, Dai and Trenberth 2004). The recent study of Dai (2006), reviewing results from 18 coupled atmosphere-ocean GCM (AOGCM) models, indicates large discrepancies involving diurnal variability of precipitation amongst the different models. Therefore, given these findings and our experience with analyzing TRMM data, it appears that modelers should improve the "diurnal processes" capabilities of their models -- including precipitation -- to ensure that they reliably simulate atmospheric circulations that themselves are diurnally modulated.

Furthermore, more detailed observational analyses of the spatiotemporal characteristics of diurnal cycle variations are needed to reveal their unique properties so that the mechanisms of the diurnal cycle can be better physically explained. Modelers would then have a better quantitative basis from which to refine model processes that control the diurnal variability of precipitation. Yang and Smith (this issue) describe the seasonal climatology of the diurnal cycle at global scales, its seasonal variability, and the contrasting behaviors of convective and stratiform components -- demonstrating that the secondary diurnal mode is largely modulated by the diurnal cycle of stratiform precipitation. In addition, Yang et al. (2006) found consistent appearance of global scale secondary precipitation maxima from eight years of TRMM data.

As a follow-up, this study demonstrates the widespread consistency in the occurrence of a secondary diurnal mode in precipitation globally, and at seasonal and regional scales. To obtain the detailed view, an innovative clock-face graphic display scheme is used to aid the analysis. Eight-year TRMM precipitation datasets derived from three level 2 TRMM standard rain rate algorithms are used to conduct the analysis. A Fourier harmonic analysis scheme is also applied to highlight the dominant diurnal modes of precipitation variability while suppressing the unimportant diurnal harmonics. The advantages, ambiguities, and pitfalls related to use of harmonic analysis are also discussed to draw attention to what can and cannot be achieved by using Fourier decomposition analysis in studying precipitation's diurnal cycle.

2. Methodology and Dataset

An "explicit" precipitation maxima selection scheme is first used to identify the primary and secondary diurnal modes at various space-time scales. A "Fourier decomposition" selection scheme is then applied as a cross-checking method and as a means to filter out ambiguous time series noise. Gridded properties of the diurnal cycle are illustrated using the clock-face display scheme. The different colors of the clock-hands denote the different diurnal modes, while the length and position of the clock-hands denote amplitude and phase characteristics of the separate diurnal modes. In addition, clock-face-colors are used to express the canonical phase interval of the primary diurnal mode.

The existence of a secondary peak in a diurnal sequence of surface precipitation rate is found using two different precipitation maxima selection schemes. The first is referred to as the "explicit" selection scheme based on logic-based detection of local relative precipitation rate maxima in a given diurnal time series. This scheme consistently identifies the appearance of either primary or secondary modes, as long as each of the separate amplitudes exceed a

minimum amplitude-emergence threshold and as long as there is sufficient separation in the positions of two detected peaks according to a second phase-angle separation threshold. Application of the "explicit" scheme may result in identification of both primary and secondary modes, only a primary mode, or no modes at all. Tertiary and quaternary modes are also identified with the "explicit" scheme.

The second scheme is referred to as the "Fourier decomposition" selection scheme. This scheme by definition identifies amplitudes and phases of all wave numbers. However, in the analysis procedure we apply, only the primary through quaternary modes are examined. It is noted that assignment of phases for the secondary through quaternary modes requires an adjustment procedure to the raw phase information for wave numbers 1 - 3 (i.e., Fourier harmonics 2 - 4). For example, in assigning the phase of a secondary mode, and defining the raw phase angles of the 1st and 2nd Fourier harmonics as ϕ_1 and ϕ_2, existence of a peak for the secondary diurnal mode is only established when each of the following two conditions is satisfied:

$$|\phi_2 - \phi_1| < 45^\circ \tag{1}$$

$$|\pi + \phi_2 - \phi_1| < 45^\circ \tag{2}$$

Thus, the peak of the 2nd harmonic is separated from the peak of the 1st harmonic by at least six hours. Otherwise, the primary and secondary modes would merge into a different primary mode with a different phase. Likewise, the phase positions of the tertiary and quaternary modes must be established by assuring appropriate phase-angle separations. As indicated earlier, the clock-face graphic display scheme can then be used to illustrate the various parameters associated with the diurnal analysis on a regular grid.

Eight-year (1998-2005) precipitation datasets derived from the three main level-2 TRMM standard precipitation algorithms are used for the study. These are the TMI-only (i.e, alg 2a12), PR-only (i.e., alg 2a25), and combined PR-TMI (i.e., alg 2b31) rain rate retrieval algorithms. The level-2 instantaneous rain rates at native orbit-swath pixel locations are first binned into eight (8) 3-hourly mean solar time (MST) bins -- then grouped at different spatial and temporal resolutions. A hierarchy of 5°x5°, 10°x10°, 20°x30° and 20°x60° latitude-longitude spatial grid resolutions are then used in processing the data at seasonal and 8-year mean temporal scales.

3. Diurnal Properties of Precipitation at Global Scale

The distribution of the 8-year mean TRMM-based precipitation diurnal cycle over oceans and continents depicts a distinct climate feature on the global scale. Figure 1 shows the climate characteristics of diurnal variability from TMI-only, PR-only, and combined PR-TMI rain rate retrievals. This diagram clearly shows that the precipitation diurnal cycles from the three TRMM rain rate products are consistent in terms of amplitude and phase over oceans, and consistent in phase over continents although with somewhat larger TMI precipitation amplitudes. Oceanic precipitation has a dominant late evening maximum in the 3-6 MST timeframe while continental precipitation has a prevailing late afternoon peak in the 15-18 MST timeframe.

Seasonal variability of the diurnal cycle is another important feature described in detail by Yang and Smith (2007). Figure 2 illustrates the climatology of seasonal variations of the diurnal cycle over oceans and continents using 8-year 2a25 PR rain rates. The primary maximum at 3-6 MST of oceanic precipitation is prominent in Spring, Autumn and Winter, but relatively weak in Summer. At the global scale, the secondary maximum over oceans is not obvious for any season. The primary late afternoon peak at 15-18 MST of continental

precipitation is the most dominant feature. The secondary late evening maximum is most apparent in Summer and Winter, while weak but detectable in Spring and Autumn.

The diurnal variations of convective and stratiform precipitation from 2a25 are also illustrated in Figure 2. Over oceans, convective precipitation exhibits the same diurnal properties as total precipitation, while stratiform precipitation exhibits a secondary peak in early afternoon in Spring and Winter in addition to its dominant late evening maximum. Over continents, the dominant late afternoon afternoon peak in convective precipitation mimics the diurnal behavior of total precipitation, while stratiform precipitation exhibits a late evening maximum at 3-6 MST and a late afternoon maximum at 15-18 MST. The TMI-only and combined PR-TMI rain rate products (figures omitted) indicate mostly similar characteristics insofar as diurnal variability.

4. Persistent Nature of Secondary Diurnal Mode

4.1 Characteristics of Secondary Mode

Horizontal distributions of the precipitation diurnal cycle based on the 8-year TRMM rain rate products analyzed on a 5°x5° grid are shown in Figure 3 illustrated in the format of clock-face grids. A blue (green) color-face of a given clock denotes a pre-noon half-day (post-noon half-day) phase interval of the dominant maximum for each grid location, where the pre-noon half-day phase interval is defined from 0-12 MST and the post-noon half-day phase interval from 12-24 MST. The transition of clock-face color is evident along almost all coastlines. This draws attention to the dominance of the pre-noon precipitation maximum over oceans (blue) and the post-noon precipitation maximum over continents (green). This behavior was reported by Yang and Smith (2006) for a one-year dataset (1998). Here it is graphically and robustly illustrated using 8 years of data at high spatial resolution at specific grid regions. It is seen that at the 5°x5°

spatial scale, a few oceanic grid locations exhibit dominant post-noon maxima, while a few continental grid locations indicate dominant pre-noon maxima. The reasons for these exceptions deserve future examination. In addition, close examination of the clock-faces reveals that secondary maxima (denoted by white inner faces) are widespread throughout the tropics and sub-tropics observed by the TRMM satellite, in which secondary post-noon peaks are found over oceans and secondary pre-noon peaks found over continents. These characteristics are highly consistent between the TMI, PR, and combined PR-TMI rain rate products.

Similar analyses conducted at 20°x30° spatial resolution scale are illustrated in Figure 4. At this grid scale, there is no ambiguity as to the separation of the primary pre-noon and post-noon modes over oceans and continents, respectively (with the proviso that the mixed land-water Maritime continent exhibits purely oceanic diurnal precipitation properties in regards to the primary mode). Note that at this grid scale, there is perfect agreement amongst the three algorithms insofar as the arrangement of the blue and green clock-faces. Also, as in Figure 3, there is widespread but not complete distribution of the secondary mode (marked by white inner clock-faces), noting that for this diurnal property, whereas there is general agreement amongst the three algorithms, there is not perfect agreement. These two aspects of the secondary mode, along with other more obscure characteristics found by close examination of the amplitudes and phases of the secondary mode (i.e., denoted by the appearances, lengths, and positions of green clock-hands) indicate that it is a more complex process than that of the primary mode. It is also apparent that the secondary mode over continents is more prevalent. Quantitatively, the results show that there is 72%, 61%, and 77% consistency in the occurrence of secondary peaks identified between the three algorithm pairings 2a12 - 2A25, 2a12 - 2b31, and 2a25 - 2b31.

Figure 5 presents another set of similar analyses, but now based only on the PR algorithm and comparing the 20°x30° result shown in Fig. 4 with results at 10°x10° and 20°x60° spatial resolutions. Although there is general agreement between the members of this set of results, there are interesting and pertinent differences pertaining to spatial resolution. First, the secondary peak is not evident over the central Pacific Ocean at the 20°x30° grid scale, but appears over this region at the 10°x10° and 5°x5° grid scales. This same effect is found over the Indian ocean and the northwest Pacific ocean subtropical regions. In addition, there are differences associated with the different horizontal scales on the occurrence of secondary maxima in the central-west Indian ocean, the central-east Pacific ocean, and north Africa.

In summarizing the effects of spatial resolution on the areal cover of the secondary mode (see Table 1), it is found that the percentage of low resolution grid positions (upper panel in Fig. 5) indicating the presence of a secondary peak is 78% (i.e., 14 of 18 grids), whereas for the medium resolution grid array (middle panel) the percentage falls to 69% (25 of 36), and then down to 65% (188 of 288) for the high resolution grid array. Based on the middle panel PR result of Fig.3 at the highest spatial resolution used in the study (i.e., 5°x5°), the percentage rises to 68% (783 of 1152). This emphasizes the sensitivity to grid resolution in evaluating the areal coverage of the secondary peak in the framework of 8-year means, with the end result being a difference of some 13% between the smallest and largest areal cover values.

Notably, when these areal cover sensitivities to spatial resolution are decomposed into differences for oceanic and continental regimes, the percentage differences become larger, which as Table 1 indicates are 30% for ocean and 16% for continents. The much larger difference for ocean is primarily due to the mixing of continental and oceanic secondary peaks at the lowest resolution. Therefore, whereas it is evident that the secondary peak in precipitation's diurnal

cycle is a widespread phenomenon over the global tropics and sub-tropics, caution must be exercised when evaluating the quantitative cover factors for oceans and continents because of the sensitivities involved. [Similar analyses using the TMI and combined PR-TMI precipitation datasets lead to almost identical percentage differences, emphasizing robustness of the results.]

Based on analyzing the 20th-century climate simulations by the newest generation of 18 coupled climate system models, Dai (2006) indicates that most climate models can reproduce general precipitation patterns and their basic annual variability, although some of these models continue to generate unrealistic double Inter-tropical Conversion Zone (ITCZ) patterns over the tropical eastern Pacific ocean -- a persisting problem in climate modeling (Mechoso et al. 1995). In addition, Dai (2006) found that most models produce too much convective precipitation and too little stratiform precipitation, resulting from unrealistically strong coupling of tropical convection to local sea surface temperatures. Most relevant to the concerns in this study, analyses of the precipitation diurnal cycle suggests that most models start to precipitate too early and too frequently at reduced intensity, showing a single late morning - early afternoon peak over continents and a single LE-EM peak over oceans. Many of these features are different from the TRMM precipitation diurnal analysis presented in this study, as well as in the Yang and Smith (2006, 2007) and Yang et al. (2006) studies.

It should come as no surprise that climate models are unable to realistically simulate the diurnal variations of precipitation. Their spatial resolutions are too low vis-à-vis precipitation physics to properly simulate the narrowly confined mass and water vapor convergence processes leading to convection or to meaningfully resolve the vertical overturnings of cloud systems that actually produce convective and stratiform precipitation fallout. Moreover, they do not have any type of meaningful microphysical parameterizations insofar as the initiation, growth, loss, phase

change, and vertical motion of either non-precipitating or precipitating hydrometeors. Thus, it is appropriate that the type of observationally-based study such as presented here, concerning highly detailed properties of precipitation processes, should be used to guide and calibrate future improvements in the embedded water cycle formulations of AOGCMs.

4.2 Convective and Stratiform Partitioning of Secondary Mode

We have demonstrated that the horizontal distribution of the primary diurnal mode of precipitation over both oceans and continents is little affected by spatial resolution. However, the spatial averaging scale imparts a significant impact on the horizontal distribution of the secondary mode. Yang and Smith (2007) show that in an 8-year averaged global framework, the secondary mode is significant over continents but weak over oceans. They also find that when considering regional-seasonal scales the secondary mode becomes significant over oceans and even more so over continents, and the different modes are largely modulated by stratiform precipitation diurnal variability. In order to explain the possible cause of this secondary mode behavior, we analyze the diurnal cycles of precipitation's convective and stratiform components.

Figure 6 illustrates the horizontal distributions of the primary and secondary diurnal cycles of precipitation from mean 8-year PR retrievals at the 20°x30° grid scale. By inspection it is evident that both convective and total precipitation exhibit the same oceanic - continental contrast in the phase of the primary diurnal peak. Also, the secondary mode of the convective component nearly mimics the secondary mode of total precipitation. Detailed inspection reveals that the phases of the dominant mode of both convective and total precipitation are approximately equivalent, however, there is a shift in phases between the secondary modes of convective and total precipitation. This shift is due to the contribution of the stratiform precipitation diurnal cycle. As seen in the lower panel of Fig. 6, an important feature is that the

dominant peak of stratiform precipitation's diurnal cycle over central Africa, Asia, Australia, and central South America occurs during the LE-EM period, while its secondary peak occurs during the MLA period at the same time as that of convective and total precipitation.

Therefore, over continents a primary LE-EM diurnal peak of stratiform precipitation is in phase with the secondary LE-EM peak of total precipitation, while convective and total precipitation exhibit similar primary MLA diurnal peaks. These results indicate that afternoon convection forced by surface solar radiative heating reaching its maximum diurnal intensity is responsible for the dominant afternoon peak of the continental precipitation diurnal cycle, i.e., the SRH mechanism. The development time of stratiform precipitation suggests that any one of a number of possible mechanisms such as the MTFPS, continental NRC-ERH, or perhaps even a SRC, DRC, or LS-VM mechanism operating within a continental environment, might explain the LE-EM maximum in stratiform precipitation, which contributes to the secondary LE-EM peak of total precipitation. In addition, the DRC mechanism operating within a continental environment might elevate nighttime precipitation while suppressing daytime precipitation -- which is how the DRC mechanism operates. These processes of convective and stratiform systems draw attention to how multiple mechanisms might compete with one another for dominance, resulting in counterpoised LE-EM and MLA modes in the continental precipitation diurnal cycle.

Over low latitude oceans, stratiform precipitation inevitably accompanies convective precipitation, especially for strong convective systems (Houze 1997). In fact, the contribution of stratiform precipitation to total accumulation is about the same as that of convective precipitation (Yang and Smith 2007). Fig. 6 actually shows that the dominant LE-EM peaks of convective and stratiform precipitation are in excellent agreement, suggesting that whatever mechanism is producing the LE-EM mode, e.g., one or more of the SRC, DRC, NRC-ERH, or LS-VM

mechanisms, is operating in synchronization with both convective and stratiform components. In addition, the secondary MLA mode, i.e., due to the OSH mechanism, is effective for both convective and stratiform precipitation diurnal variability, although close inspection of Fig. 6 suggests that the modulation of the ocean's secondary mode amplitude stems mostly from fluctuations in the amplitude of the stratiform component. Similar analyses conducted at higher spatial resolutions lead to similar findings for the primary peak of the diurnal cycle, while the secondary peak exhibits somewhat more complex behavior (figure omitted). The secondary mode intermittently spreads out over the entire tropics and subtropics at the 5°x5° grid scale. Over oceans, this behavior suggests that the secondary MLA mode is more important at smaller horizontal scales.

5. Harmonic Analysis of Diurnal Cycle

5.1 Diurnal Characteristics Revealed from Harmonic Analysis

A Fourier harmonic decomposition scheme is applied to examine the diurnal variability of precipitation in order to elucidate the foremost amplitude and phase features while filtering high frequency noise. Because this approach suppresses spurious variations in a diurnal time series that might be detected as extrema in the explicit method, it is worthwhile evaluating its worth. Figure 7 compares the horizontal distribution of the precipitation diurnal cycle based on the explicit scheme applied to 5°x5° gridded PR-only retrievals over the 8-year (1998-2005) time period, to a counterpart result based on application of the Fourier decomposition scheme. The clock-face plots provide all essential details concerning amplitudes and phases, for not only the primary and secondary modes, but also for tertiary and quaternary modes. Colors and clock-hand pointing denote phase information while clock-hand length denotes amplitude information.

A strong contrast between primary harmonic diurnal phases over oceans and continents is the eye-catching feature in the upper panel of Fig. 7 (explicit scheme) as it is in the middle panel (Fourier decomposition scheme). The clear-cut contrast between the oceanic LE-EM phase and continental-like MLA phase along coastlines is actually sharper in the middle panel than in the upper panel. In addition, there are fewer spurious regions in the middle panel where the primary precipitation peaks are misidentified. A four-color clock-face scheme showing a more detailed representation of the phase interval of the primary mode is shown in the lower panel. Over oceans, frequent occurrence of late evening interval (0-6 MST) peaks is the dominant diurnal feature, with additional occurrences of morning interval (6-12 MST) peaks largely over coastal regions. Over continents, the occurrence of early evening interval (18-24 MST) peaks is the dominant feature over Africa and Australia, while the afternoon interval (12-18 MS) peaks are dominant over South America, North America and Asia. These more detailed diurnal features suggest that either different mechanisms are at work or singular mechanisms dominate but are dispersive in their timing of the maxima within different environments. Similar analyses at lower spatial resolution confirms that the underlying spatial distribution patterns of primary and secondary modes, as seen in Fig. 7, are not greatly affected by the use of a high resolution scale.

The higher order harmonic modes conform to semi-diurnal, tri-diurnal, and quartic-diurnal variations, and require an interpretation of where to position the actual peaks in terms of their phase angles in time. Figure 8 presents a comparison of the first three principal diurnal modes based on use of the explicit scheme in the upper panel, and the first two principal Fourier harmonics in the lower panel cast onto 20°x30° grids. The clock-face color exhibits a pre-noon half-day phase interval (blue) and post-noon half-day phase interval (green) of the primary diurnal mode. The secondary modes are shown by use of white inner clock-faces. It is obvious

that the horizontal distribution of the primary diurnal mode based on use of the explicit scheme is consistent with the horizontal distribution of the same mode based on use of the Fourier decomposition scheme, although close inspection of the two diagrams shows that small phase differences occur. More relevant are the greater and more frequent differences concerning both amplitudes and phases of the secondary mode between the two maxima identification schemes.

The secondary mode will appear almost everywhere with Fourier analysis, simply because even if there is no secondary peak in actuality, almost invariably some power will leak into wave number 2. Even though it does not satisfy the definition of the secondary mode over the northern part of South America and central South Africa, the secondary mode from the Fourier decomposition scheme is still apparent over these areas in comparison with the explicit scheme. For those grid positions where only a primary mode is found from the explicit scheme (such as over the central Pacific Ocean and the west Indian Ocean), a secondary mode is often identified from the Fourier analysis. The sources of the ambiguities associated with Fourier harmonic analysis of precipitation's diurnal cycle are discussed in the next section.

5.2 Ambiguities Associated with Harmonic Analysis

The results presented in the previous section demonstrate that the Fourier decomposition approach is robust for the primary diurnal mode of precipitation, especially the phase of the dominant diurnal peak -- as noted in, for example, the Collier and Bowman (2004) and Yang and Smith (2006) studies. However, the nature of Fourier harmonic analysis can lead to misinterpretation of both amplitudes and phases of different modes as they mix together, even the mixing of perfect sinusoidal modes. This can be especially problematic in seeking to identify and describe a secondary diurnal mode. Thus, ambiguities are inevitable when using Fourier analysis in analyzing precipitation's diurnal variability. These ambiguities arise from a number

of sources. Of necessity, diurnal precipitation modes are: (a) generally truncated semi-diurnal modes, (b) represented as repeating cycles over the 24-hour diurnal period for wave number 1 and beyond, and (c) not purely sinusoidal and thus dispersive in their power spectrum over a spread of frequencies when considering realistic diurnal modes in actual observations.

Figure 9 demonstrates a case of Fourier decomposition for 2 purely sinusoidal, but truncated, diurnal modes with equal amplitude but shifted phase. The 2 peaks occur in early morning and late afternoon. The original components and combined time series for the double-peak cycle are illustrated in the left 3 panels. The right 4 panels present their successive reconstructed diurnal cycles using the mean and first 3 principal Fourier harmonics. Note that the primary mode is the 2nd harmonic (wave number 2) which produces 2 diurnal peaks. Along with the mean value (wave number 0), the primary mode reproduces the basic diurnal properties but with a phase shift. Inclusion of the secondary mode (i.e., 1st harmonic, wave number 1) produces a more realistic time series in which both amplitudes and phases are near their original values. However, it is evident that at least 3 harmonics are needed to reconstruct a sound representation of the original combined time series -- based on the mixing of 2 perfect, but truncated, sinusoids.

A similar analysis is conducted for another case in which the amplitude of the late afternoon peak is much smaller than that of the early morning peak (Figure 10). The primary mode (1st harmonic, wave number 1) depicts nicely the phase of the principal diurnal peak, however, its amplitude is too small compared with the original value. Furthermore, the single primary harmonic cannot reproduce the secondary late afternoon peak. It is evident that the reconstructed diurnal cycle produced by the inclusion of the 2nd harmonic (wave number 2) produces a realistic primary early morning peak in both amplitude and phase, as well as a

realistic secondary late afternoon peak in amplitude but with a phase shift. Thus, a 3rd harmonic is needed to bring about a reconstructed diurnal cycle that is similar to the original.

Figure 11 presents a final case, but now for a realistic observational situation, with a dominant peak at noon and a weaker secondary peak in late afternoon. Additional higher frequency fluctuations are also evident -- which can be considered either real data properties, or more often noise due to retrieval error and/or under-sampling. Clearly, the harmonic approach can be used to eliminate the high frequency waves. In reconstruction, the primary mode (1st harmonic, wave number 1) clearly reproduces the phase of the dominant peak, although the weak secondary peak is missed. Due to the small phase separation between the dominant primary peak and weak secondary peak, the 3rd harmonic (wave number 3) represents the secondary mode. Using only the first two principal harmonics, the reconstructed diurnal cycle exhibits the basic features of the original cycle, however, with a discernible phase shift in the secondary mode.

There are two main points to this analysis. First, when using the Fourier decomposition scheme, the dominant harmonic (along with the mean value), are able to reproduce the main features of the primary diurnal peak, particularly its phase. Second, the mean and first two principal harmonics generally can reproduce some, but not all, of the key features of the secondary peak. For some cases, the dominant harmonic cannot adequately reproduce the amplitude and/or phase features of the primary mode -- but for the TRMM data we have analyzed, these occurrences only arise ~6% of the time. Thus, since the diurnal cycle of precipitation often has a dominant primary peak and a weaker secondary peak, the principal Fourier harmonic is used to represent the main features of the strong primary mode, while the second harmonic is used to represent the main features of the weak secondary mode. In doing so, it must be recognized that a phase shift is often associated with the representation of the

secondary mode, as well as possible amplitude errors for both modes. Note, the second harmonic is often needed to contribute to the amplitude behavior of the primary mode. Finally note, the harmonic approach can bring about a false secondary mode when only a single primary mode is present, in considering the case when a second harmonic is used to compensate for amplitude misrepresentation in the primary mode.

Therefore, caution is always required in identifying secondary modes when using the Fourier decomposition scheme. Background knowledge of regional precipitation properties is always helpful in mitigating against ambiguities caused by applying harmonic analysis. In terms of our secondary mode analyses with TRMM precipitation data, the incidences of mis-interpretation associated with the Fourier decomposition scheme are relatively frequent, particularly for the higher spatial resolutions, contaminating the results some 45% of the time.

6. Discussion and Conclusions

This study has examined the diurnal variability of precipitation at various spatial and temporal scales based on 8-year TRMM TMI, PR, and combined PR-TMI precipitation datasets. We find that these three distinct rain rate products produce consistent behavior insofar as the diurnal cycle properties of precipitation. The 8-year averaged diurnal cycles of oceanic and continental precipitation consistently exhibit primary maxima during the 3-6 MST and 15-18 MST periods, respectively. Moreover, counterpart secondary maxima are strongly evident throughout the global tropics and sub-tropics, with seasonal variation being a very prominent feature of the secondary mode. These outstanding features of the diurnal behavior of oceanic and continental precipitation on a global scale are presented by use of a specially-designed graphic made up of gridded clock-faces with clock-hands, and coloring techniques to simultaneously display the various key parameters of harmonically complex precipitation

variation at the diurnal time scale. The secondary precipitation maxima generally consist of afternoon peaks over oceans and morning peaks over continents. Notably, this is the first study in which the widespread secondary mode has been identified and given special attention.

It is important to recognize that based on our past and current TRMM data analyses, we find that the secondary maxima are largely produced and modulated by stratiform precipitation (see Yang and Smith 2007). Although we have shown that the underlying properties of the precipitation diurnal cycle are influenced by the spatial and temporal resolutions at which the data are analyzed, we find that there is a great deal of consistency in how oceanic and continental regions contrast with one another, regardless of the underlying resolutions. For example, the impact of spatial resolution is generally not significant concerning the primary diurnal mode, although it can be significant in identifying the areal coverage of the secondary diurnal mode. Most importantly, the global distribution of the precipitation diurnal cycle exhibits considerable seasonal variations -- largely due to the occurrence of secondary diurnal modes.

The Fourier decomposition scheme does a credible job in identifying the main amplitude and phase features of the primary mode with the advantage of eliminating spurious high frequency fluctuations in the original diurnal time series. We find that this approach is at its best when representing the phase of the primary diurnal mode. Nonetheless, at times, secondary, tertiary, and even quaternary modes are needed in reproducing realistic amplitudes of the primary mode. Thus, the Fourier decomposition scheme can produce isolated ambiguities vis-à-vis the interpretation of the primary diurnal mode, depending on how the scheme is applied.

Furthermore, we have demonstrated how and why the Fourier decomposition scheme creatse ambiguities in representing the amplitude and phase properties of the secondary diurnal mode because of the up-frequency mixing of power from the first principal mode into the higher

order modes. We have shown that secondary diurnal modes over some regions derived from the Fourier scheme applied to TRMM data -- are simply not real. Therefore, caution is in order when interpreting the amplitudes and phases of the secondary, tertiary, and quaternary modes, apart from any coherency at the global scale, when using Fourier analysis -- noting that ambiguities in representing the secondary mode are unavoidable. Nonetheless, surface precipitation normally exhibits fairly distinct primary and secondary diurnal peaks such that the Fourier decomposition scheme is often applicable. In any case, background knowledge of the pertinent meteorological variables controlling precipitation, as well as understanding how the precipitation variables behave in response to the relevant diurnal mechanisms at work, are always helpful in analyzing for secondary diurnal modes when using Fourier decomposition.

7. Acknowledgments

The authors gratefully acknowledge staff members of the TRMM Science Data and Information System (TSDIS) for providing the datasets used in this study. This research was supported by Dr. Ramesh Kakar at NASA Headquarters in conjunction with the Precipitation Measurement Missions (PMM) Science Team research program.

8. References

Anderson, S. P., R. A. Weller, and R. B. Lukas, 1996: Surface buoyancy forcing and the mixed layer of the western Pacific warm pool: Observation and one-dimensional model results. *J. Clim.*, **9**, 3056-3085.

Augustine, J. A., 1984: The diurnal variation of large-scale inferred rainfall over the tropical Pacific Ocean during 1979. *Mon. Wea. Rev.*, **112**, 1745-1751.

Chen, T.-C., M.-C. Yen, J.-C. Hsieh, and R. W. Arritt, 1999: Diurnal and seasonal variations of the rainfall measured by the automatic rainfall and meteorological telemetry system in Taiwan. *Bull. Amer. Meteor. Soc.*, **80**, 2299–2312.

Collier, J. C., and K. P. Bowman, 2004: Diurnal cycle of tropical precipitation in a general circulation model. *J. Geophys. Res.*, **109**, D17105, doi:10.1029/2004JD004818.

Dai, A., 2001: Global precipitation and thunderstorm frequencies. Part II: Diurnal variations. *J. Clim.*, **14**, 1112-1128.

Dai, A., and K. E. Trenberth, 2004: The diurnal cycle and its depiction in the Community Climate System Model. *J. Clim.*, **17**, 930-951.

Dai, A., 2006: Precipitation characteristics in eighteen coupled climate models. *J. Clim.*, **19**, 4605-4630.

Deser, C., and C. A. Smith, 1998: Diurnal and semidiurnal variations of the surface wind field over the tropical Pacific ocean. *J. Clim.*, **11**, 1730-1748.

Fu, R., A. D. Del Genio, and W. B. Rossow, 1990: Behavior of deep convective clouds in the tropical Pacific from ISCCP radiances. *J. Clim.*, **3**, 1129-1152.

Gray, W. M., and R. W. Jacobson, Jr., 1977: Diurnal variation of deep cumulus convection. *Mon. Wea. Rev.*, **105**, 1171-1188.

Hann, J., 1901: *Lehrbuch der Meteorologie* (1st ed). Chr. Herm Tachnitz, Leipzig, 338-346.

Hong, Y., K.-L. Hsu, S. Sorooshian, and X. Gao, 2005: Improved representation of diurnal variability of rainfall retrieved from the Tropical Rainfall Measurement Mission Microwave Imager adjusted Precipitation Estimation From Remotely Sensed Information Using Artificial Neural Networks (PERSIANN) system. *J. Geophys. Res.*, **110**, doi:10.1029/2004JD005301.

Houze, R. A., Jr., 1997: Stratiform precipitation in regions of convection: A meteorological paradox. *Bull. Amer. Meteor. Soc.*, **78**, 2179-2196.

Krishnamurti, T. N., and C. M. Kishtawal, 2000: A pronounced continental-scale diurnal mode of the Asian summer monsoon. *Mon. Wea. Rev.*, **128**, 462-473.

McBride, J. L., and W. M. Gray, 1980: Mass divergence in tropical weather systems. Part I: Diurnal variation. *Quart. J. Roy. Meteor. Soc.*, **106**, 501-516.

McGarry, M. M., and R. J. Reed, 1978: Diurnal variations in convective activity and precipitation during Phases II and III of GATE. *Mon. Wea. Rev.*, **106**, 101-113.

Mechoso, C. R., A. W. Robertson, N. Barth, M. K. Davey, P. Delecluse, P. R. Gent, S. Ineson, B. Kirtman, M. Latif, H. Le Treut, T. Nagai, J. D. Neelin, S. G. H. Philander, J. Polcher, P. S. Schopf, T. Stockdale, M. J. Suarez, L. Terray, O. Thual, and J. J. Tribbia, 1995: The seasonal cycle over the tropical Pacific in coupled ocean-atmosphere general circulation models. *Mon. Wea. Rev.*, **123**, 2825–2838.

Oki, T., and K. Musiaki, 1994: Seasonal change of the diurnal cycle of precipitation over Japan and Malaysia. *J. Appl. Meteor.*, **33**, 1445-1463.

Petenko, I. V., and S. Argentini, 2002: The annual behavior of the semidiurnal and diurnal pressure variations in East Antarctica. *J. Appl. Meteor.*, **41**, 1093-1100.

Pielke, R. A., 2002: *Mesoscale Meteorological Modeling* (2nd ed.). Academic Press, New York, 676 pp.

Ramage, C. S., 1971: *Monsoon Meteorology*. Academic Press, New York, 295 pp.

Randall, D. A., Harshvardhan, and D. A. Dazlich, 1991: Diurnal variability of the hydrologic cycle in a general circulation model. *J. Atmos. Sci.*, **48**, 40-62.

Reed, R. J., and K. D. Jaffe, 1981: Diurnal variation of summer convection over West Africa and the tropical eastern Atlantic during 1974 and 1978. *Mon. Wea. Rev.*, **109**, 2527-2534.

Schwartz, B. E., and L. F. Bosart, 1979: The diurnal variability of Florida rainfall. *Mon. Wea. Rev.*, **107**, 1535–1545.

Serra, Y. L., and M. J. McPhaden, 2004: In situ observations of diurnal variability in rainfall over the tropical Pacific and Atlantic oceans. *J. Clim.*, **17**, 3496–3509.

Smith, E.A., 1986: The structure of the Arabian heat low. Part I: Surface energy budget. *Mon. Wea. Rev.*, **114**, 1067-1083.

Smith, E.A., E.R. Reiter, and Y. Gao, 1986: Transition of the surface energy budget in the Gobi desert between spring and summer seasons. *J. Clim. Appl. Meteor.*, **25**, 1725-1740.

Smith, E.A., and L. Shi, 1992: Surface forcing of the infrared cooling profile over Tibetan Plateau. Part I: Influence of relative longwave radiative heating at high altitude. *J. Atmos. Sci.*, **49**, 805-822.

Smith, G. L., and D. A. Rutan, 2003: The diurnal cycle of outgoing longwave radiation from Earth Radiation Budget Experiment measurements. *J. Atmos. Sci.*, **60**, 1529-1542.

Sui, C.-H., K.-M. Lau, Y. N. Takayabu, and D. A. Short, 1997: Diurnal variations in tropical oceanic cumulus convection during TOGA COARE. *J. Atmos. Sci.*, **54**, 639-655.

Sui, C.-H., K.-M. Lau, and X. Li, 1998: Convective-radiative interaction in simulated diurnal variations of tropical cumulus ensemble. *J. Atmos. Sci.*, **55**, 2345-2357.

Tao, W.-K., S. Lang, J. Simpson, C.-H. Sui, B. Ferrier, and M.-D. Chou, 1996: Mechanisms of cloud-radiation interaction in the tropics and midlatitudes. *J. Atmos. Sci.*, **53**, 2624-2651.

Wylie, D. P., and H. M. Woolf, 2002: The diurnal cycle of upper-tropospheric clouds measured by GOES-VAS and the ISCCP. *Mon. Wea. Rev.*, **130**, 171-179.

Yang, S., and E. A. Smith, 2006: Mechanisms for diurnal variability of global tropical rainfall observed from TRMM. *J. Clim.*, **19**, 5190–5226.

Yang, S., E.A. Smith, and K.-S. Kuo, 2006: Diurnal variability of precipitation from TRMM measurements. *Remote Sensing and Modeling of the Atmosphere, Oceans, and Interactions* [T. N. Krishnamurti, B. N. Goswami, and T. Iwasaki, eds.], *Proc. SPIE*, **6404**, 64040I1-6.

Yang, S., and E. A. Smith, 2007: Convective - stratiform precipitation variability at seasonal scale from eight years of TRMM observations: Implications for multiple modes of diurnal variability. *J. Clim.*, submitted.

List of Tables

Table 1: Areal coverage of secondary peak in diurnal precipitation cycle (given in %) at various spatial resolutions. [Results based on TRMM PR measurements.]

	5°x5°	10°x10°	20°x30°	20°x60°
Continental Regime	68	64	85	80
Oceanic Regime	69	65	55	85
Total	68	65	69	78

List of Figures

Figure 1: Mean diurnal cycles of oceanic (left panel) and continental (right panel) precipitation from eight years (1998-2005) of TRMM satellite data based on TMI (2a12), PR (2a25), and combined PR-TMI (2b31) TRMM standard algorithm retrievals. [Key to both diagrams given in left panel.]

Figure 2: Mean diurnal cycles of seasonal precipitation from PR algorithm retrievals for eight years (1998-2005) over oceans (left panels) and continents (right panels). Total, convective, and stratiform precipitation classifications are denoted by T, C, and S, respectively. [Key to all diagrams given in upper-left panel.]

Figure 3: Horizontal distributions of diurnal precipitation cycles based on TRMM satellite data averaged over 8-year period (1998-2005) and analyzed on 5°x5° spatial grids -- using clock-face diagrams. Upper, middle, and lower panels provide results for TMI, PR, and combined PR-TMI algorithms, respectively. North, east, south, and west points of given clock-face refer to 00, 06, 12, and 18 MST phases, respectively. Blue clock-face indicates that primary mode occurs some time during pre-noon half-day (0-12 MST) phase interval, while green clock-face indicates that primary mode occurs some time during post-noon half-day (12-24 MST) phase interval. Black upper half-circle of each clock-face denotes nighttime period, while white lower half-circle denotes daytime period. White inner clock-face highlights grid position where secondary diurnal maximum is clearly evident. Red clock-hand points to numeric phase of primary mode, green hand of secondary mode, and blue hand of tertiary mode -- over 0-24 MST interval. Amplitude of individual mode is denoted by length of associated clock-hand, in which four embedded rings indicate magnitudes (on log scale) of 0.15, 0.3, 1.5, and 3 mm day^{-1}.

Figure 4: Same as in Fig. 3, except that results are analyzed on 20°x30° spatial grids such that rows represent 10-30°S, 10°S-10°N, and 10-30°N latitude belts.

Figure 5: Same as in Fig. 3, except for only PR algorithm with separate panels illustrating results on 20°x60° (upper), 20°x30° (middle), and 10°x10° (lower) grids.

Figure 6: Same as in Fig. 4, except for only PR algorithm with separate panels illustrating results for total (upper), convective (middle), and stratiform (lower) precipitation.

Figure 7: Comparison of horizontal distributions of PR algorithm-based precipitation diurnal cycles involving two different maxima identification schemes applied in 8-year averaging framework (1998-2005) on 5°x5° grids -- using clock-face diagrams. Upper panel shows dominant maxima based on "explicit" scheme. Middle and lower panels show first four dominant maxima based on "Fourier decomposition" scheme -- using two different clock-face color formats for indicating modal phase intervals (1^{st} of these formats is same as used for upper panel). Two-color clock-face format is used for upper and middle panels, in which blue clock-face denotes that primary mode occurs some time during pre-noon half-day (0-12 MST) phase interval, while green clock-face denotes that primary mode occurs some time during post-noon half-day (12-24 MST) phase interval. Four-color clock-face format is used for lower panel, in which blue, light blue, green, and light green faces denote that primary mode occurs some time during late evening (0-6 MST), morning (6-12 MST), afternoon (12-18 MST), or early evening (18-24 MST) phase interval, respectively. Red clock-hand indicates numeric phase of primary harmonic, green hand of secondary harmonic, blue hand of tertiary harmonic, and black hand of quaternary harmonic -- over 0-24 MST interval. Amplitude of individual mode is denoted by length of associated clock-hand, in which four embedded rings indicate magnitudes (on log scale) of 0.15, 0.3, 1.5, and 3 mm day^{-1}.

Figure 8: Same as in Fig. 7, except for: (a) application on only two 20°x30° grids, (b) use of only two-color clock-face format, (c) extraction of only first three principal modes for explicit scheme, (d) extraction of only first two principal harmonics for Fourier decomposition scheme, and (e) use of white inner clock-face to denote grid position where secondary diurnal maximum is clearly evident.

Figure 9: Fourier decomposition of two purely sinusoidal, but truncated, equal-amplitude and phase-shifted diurnal modes combined into two-peak diurnal cycle. Three left-hand panels show two separate diurnal modes along with combined diurnal cycle. Four right-hand panels show successive reconstructions of combined diurnal cycle using mean value (wave number 0) and first three principal Fourier harmonics (wave numbers 1 - 3).

Figure 10: Same as in Fig. 9, except that two diurnal modes are unequal-amplitude.

Figure 11: Same as in Fig. 9, except that two diurnal modes are realistic (non-sinusoidal and unequal-amplitude).

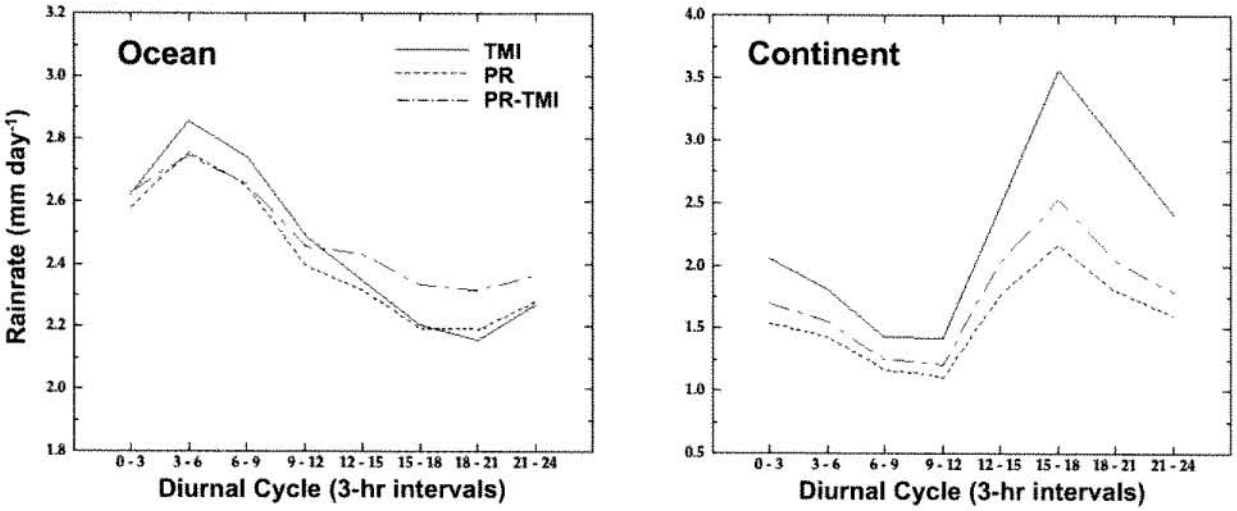

Figure 1: Mean diurnal cycles of oceanic (left panel) and continental (right panel) precipitation from eight years (1998-2005) of TRMM satellite data based on TMI (2a12), PR (2a25), and combined PR-TMI (2b31) TRMM standard algorithm retrievals. [Key to both diagrams given in left panel.]

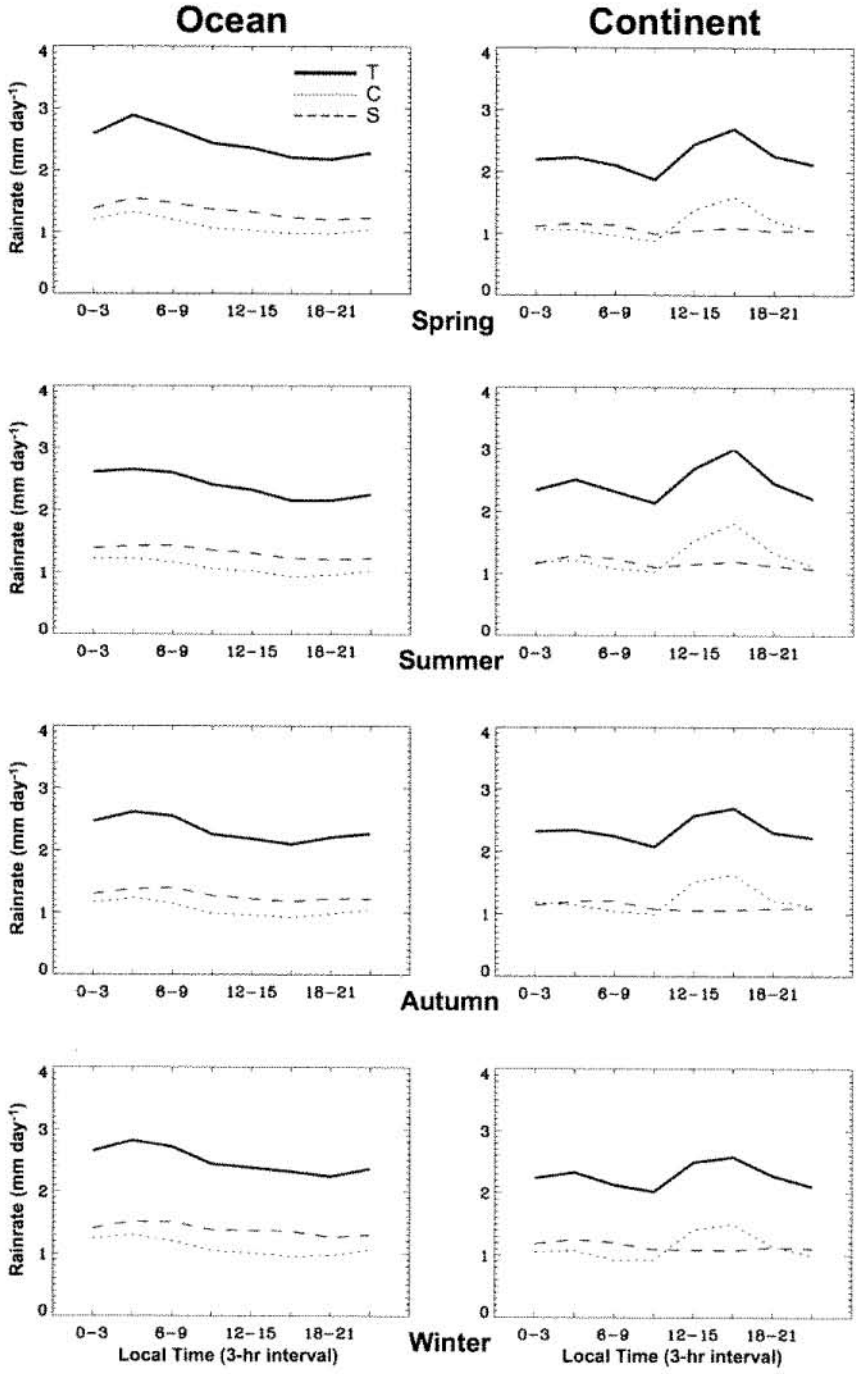

Figure 2: Mean diurnal cycles of seasonal precipitation from PR algorithm retrievals for eight years (1998-2005) over oceans (left panels) and continents (right panels). Total, convective, and stratiform precipitation classifications are denoted by T, C, and S, respectively. [Key to all diagrams given in upper-left panel.]

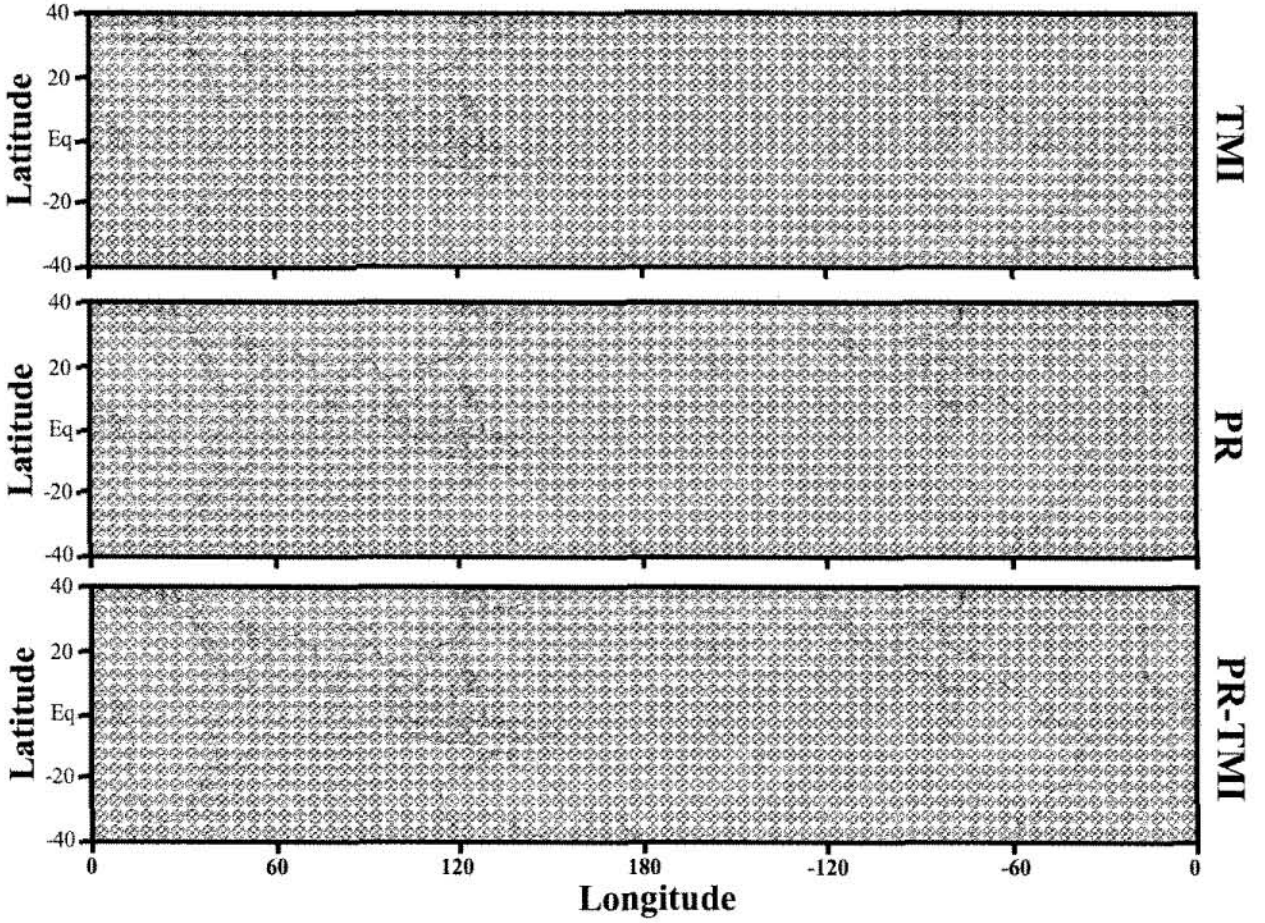

Figure 3: Horizontal distributions of diurnal precipitation cycles based on TRMM satellite data averaged over 8-year period (1998-2005) and analyzed on 5°x5° spatial grids -- using clock-face diagrams. Upper, middle, and lower panels provide results for TMI, PR, and combined PR-TMI algorithms, respectively. North, east, south, and west points of given clock-face refer to 00, 06, 12, and 18 MST phases, respectively. Blue clock-face indicates that primary mode occurs some time during pre-noon half-day (0-12 MST) phase interval, while green clock-face indicates that primary mode occurs some time during post-noon half-day (12-24 MST) phase interval. Black upper half-circle of each clock-face denotes nighttime period, while white lower half-circle denotes daytime period. White inner clock-face highlights grid position where secondary diurnal maximum is clearly evident. Red clock-hand points to numeric phase of primary mode, green hand of secondary mode, and blue hand of tertiary mode -- over 0-24 MST interval. Amplitude of individual mode is denoted by length of associated clock-hand, in which four embedded rings indicate magnitudes (on log scale) of 0.15, 0.3, 1.5, and 3 mm day^{-1}.

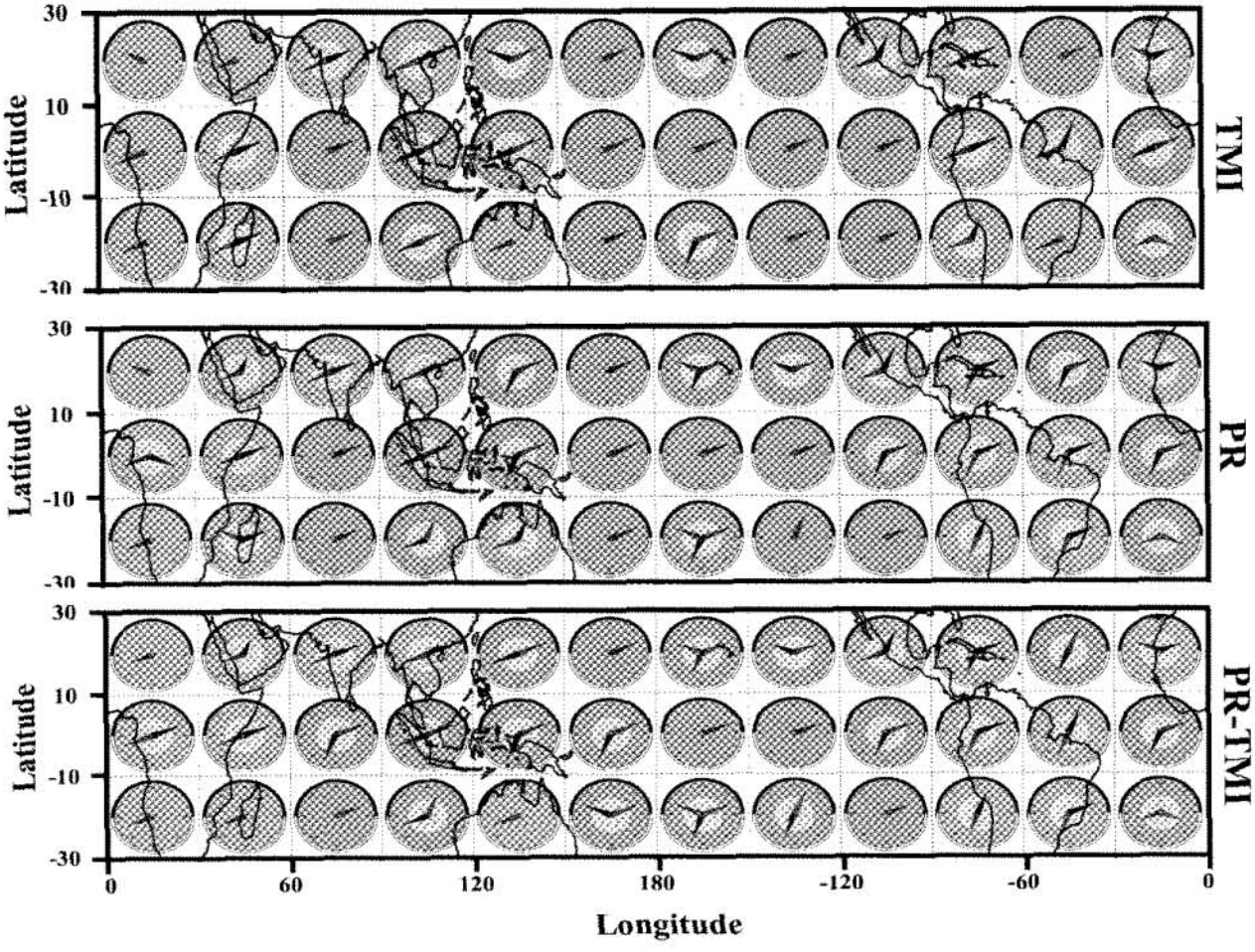

Figure 4: Same as in Fig. 3, except that results are analyzed on 20°x30° spatial grids such that rows represent 10-30°S, 10°S-10°N, and 10-30°N latitude belts.

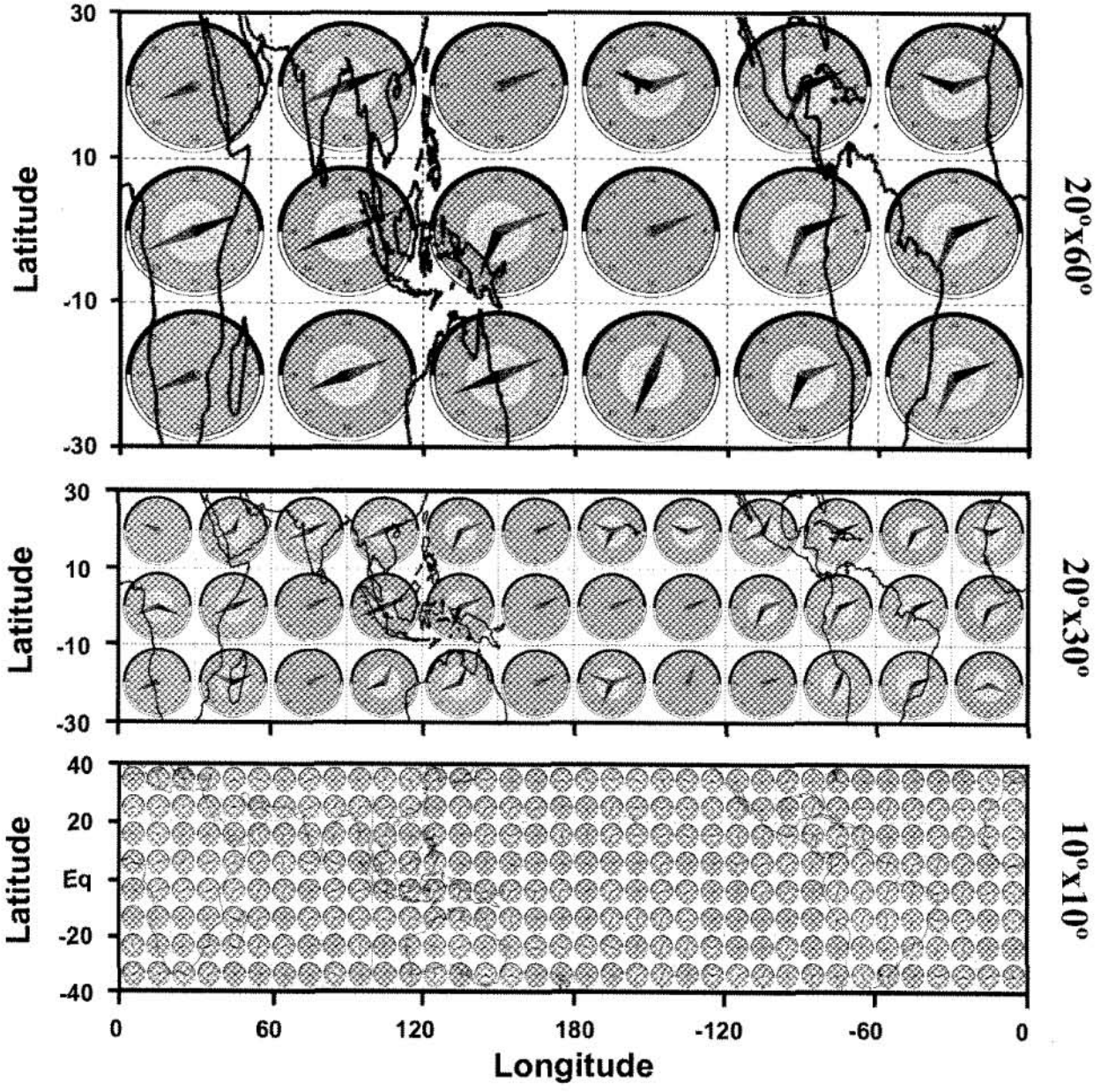

Figure 5: Same as in Fig. 3, except for only PR algorithm with separate panels illustrating results on 20°x60° (upper), 20°x30° (middle), and 10°x10° (lower) grids.

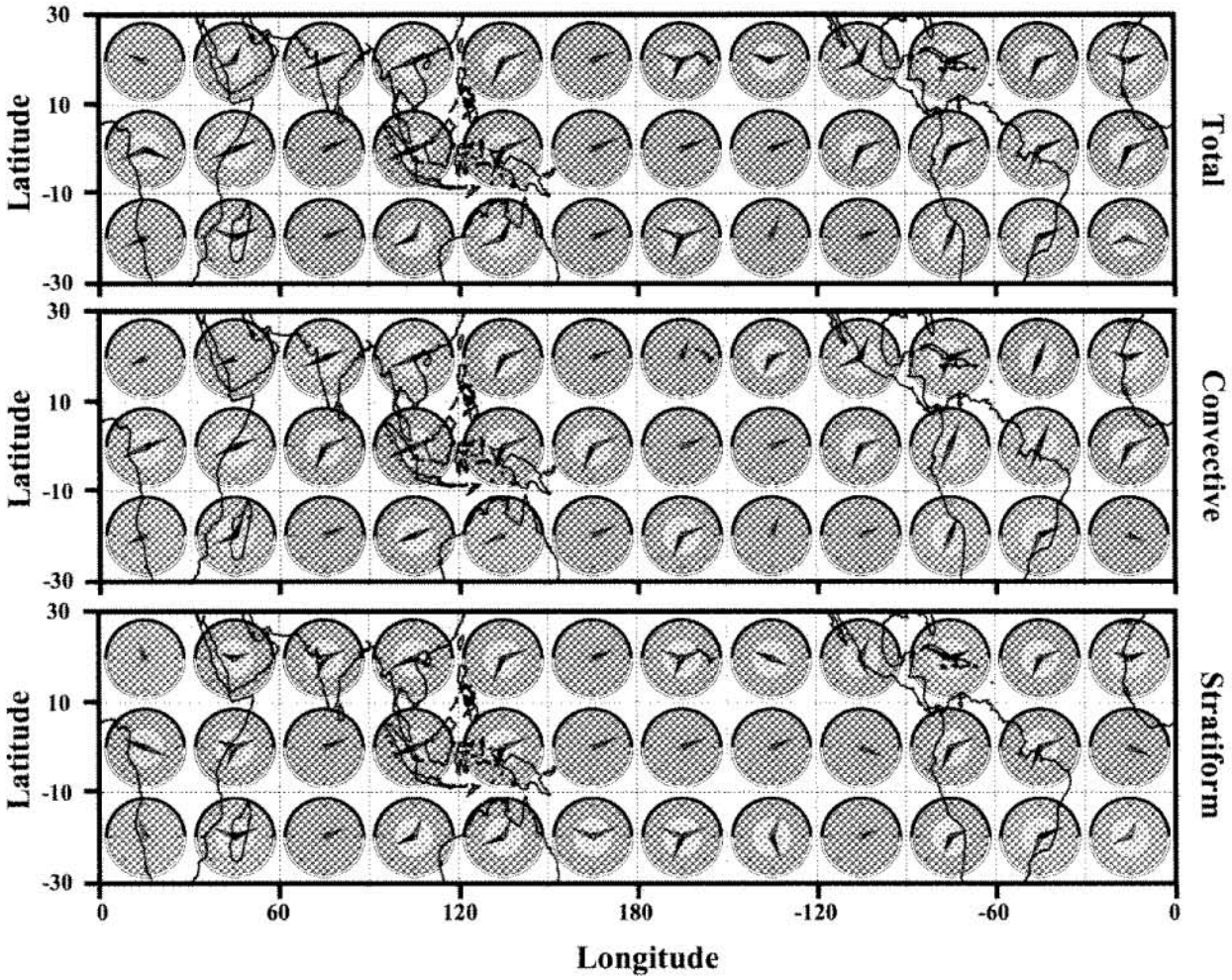

Figure 6: Same as in Fig. 4, except for only PR algorithm with separate panels illustrating results for total (upper), convective (middle), and stratiform (lower) precipitation.

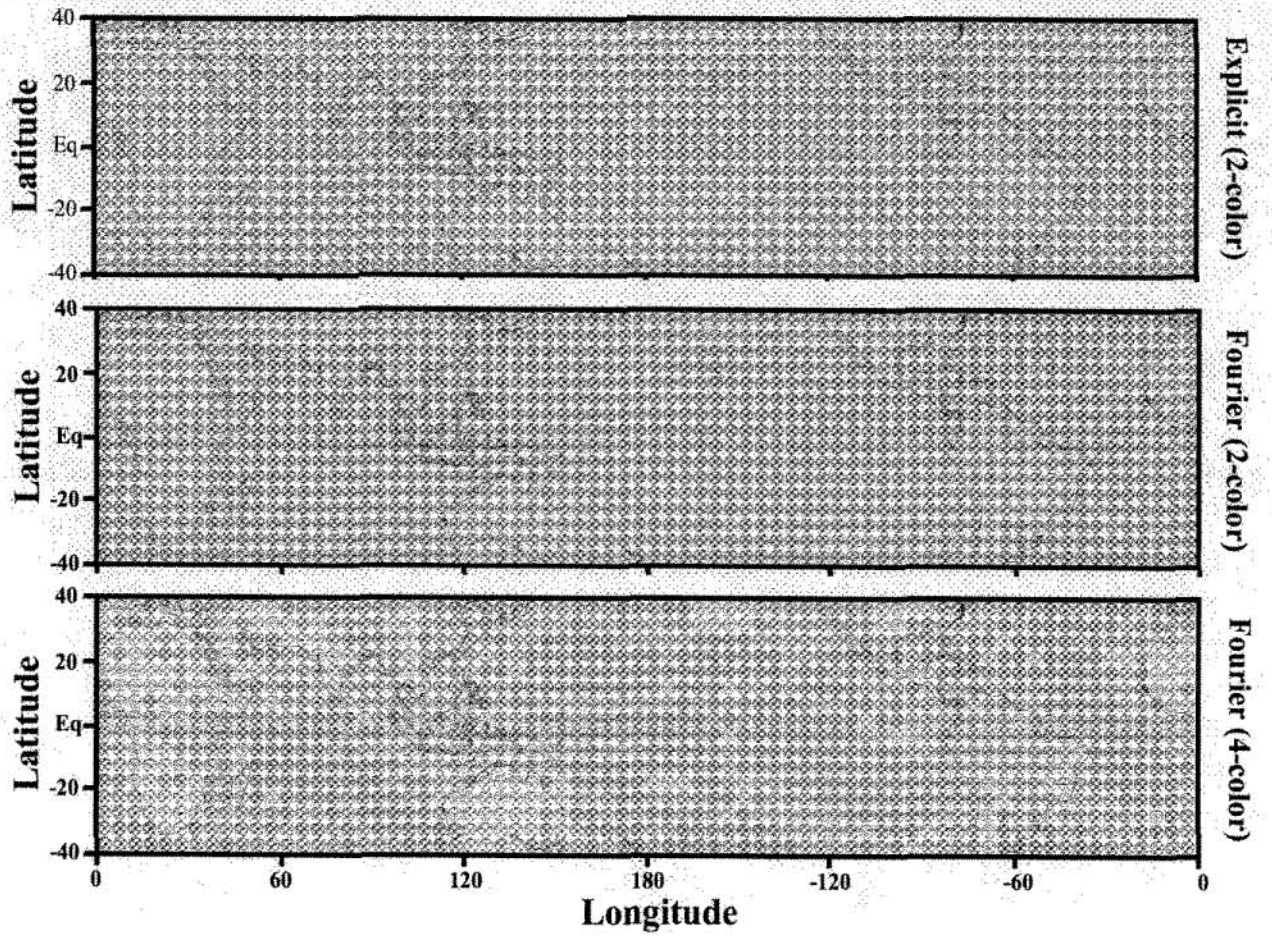

Figure 7: Comparison of horizontal distributions of PR algorithm-based precipitation diurnal cycles involving two different maxima identification schemes applied in 8-year averaging framework (1998-2005) on 5°x5° grids -- using clock-face diagrams. Upper panel shows dominant maxima based on "explicit" scheme. Middle and lower panels show first four dominant maxima based on "Fourier decomposition" scheme -- using two different clock-face color formats for indicating modal phase intervals (1^{st} of these formats is same as used for upper panel). Two-color clock-face format is used for upper and middle panels, in which blue clock-face denotes that primary mode occurs some time during pre-noon half-day (0-12 MST) phase interval, while green clock-face denotes that primary mode occurs some time during post-noon half-day (12-24 MST) phase interval. Four-color clock-face format is used for lower panel, in which blue, light blue, green, and light green faces denote that primary mode occurs some time during late evening (0-6 MST), morning (6-12 MST), afternoon (12-18 MST), or early evening (18-24 MST) phase interval, respectively. Red clock-hand indicates numeric phase of primary harmonic, green hand of secondary harmonic, blue hand of tertiary harmonic, and black hand of quaternary harmonic -- over 0-24 MST interval. Amplitude of individual mode is denoted by length of associated clock-hand, in which four embedded rings indicate magnitudes (on log scale) of 0.15, 0.3, 1.5, and 3 mm day^{-1}.

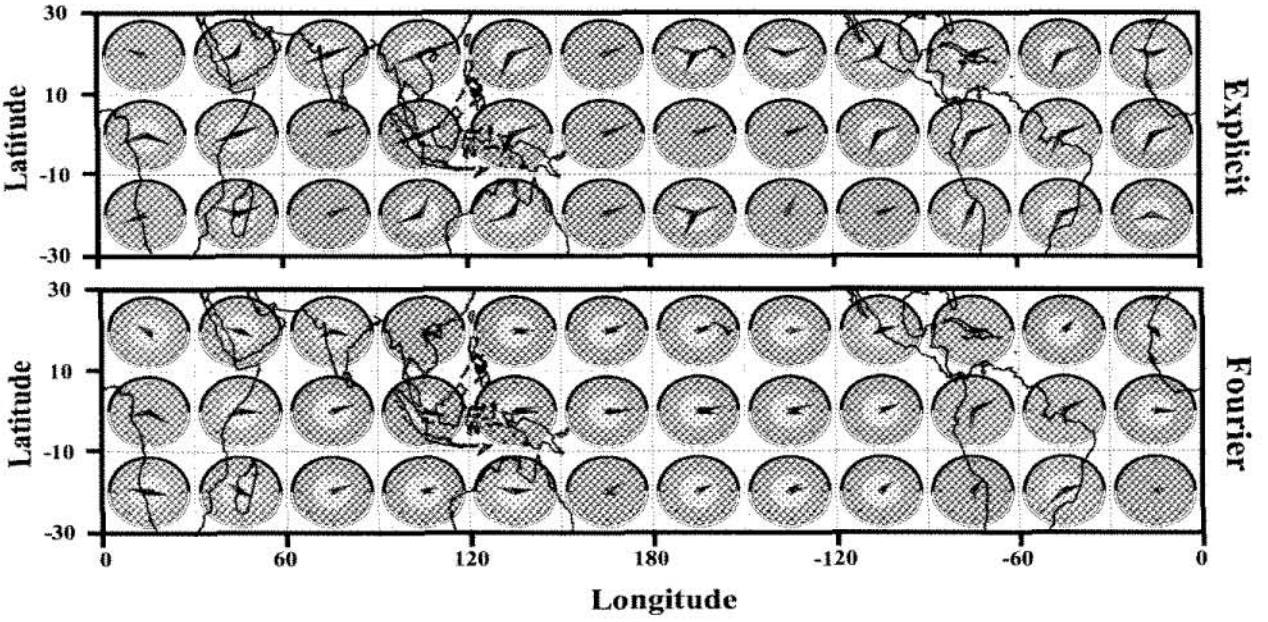

Figure 8: Same as in Fig. 7, except for: (a) application on only two 20°x30° grids, (b) use of only two-color clock-face format, (c) extraction of only first three principal modes for explicit scheme, (d) extraction of only first two principal harmonics for Fourier decomposition scheme, and (e) use of white inner clock-face to denote grid position where secondary diurnal maximum is clearly evident.

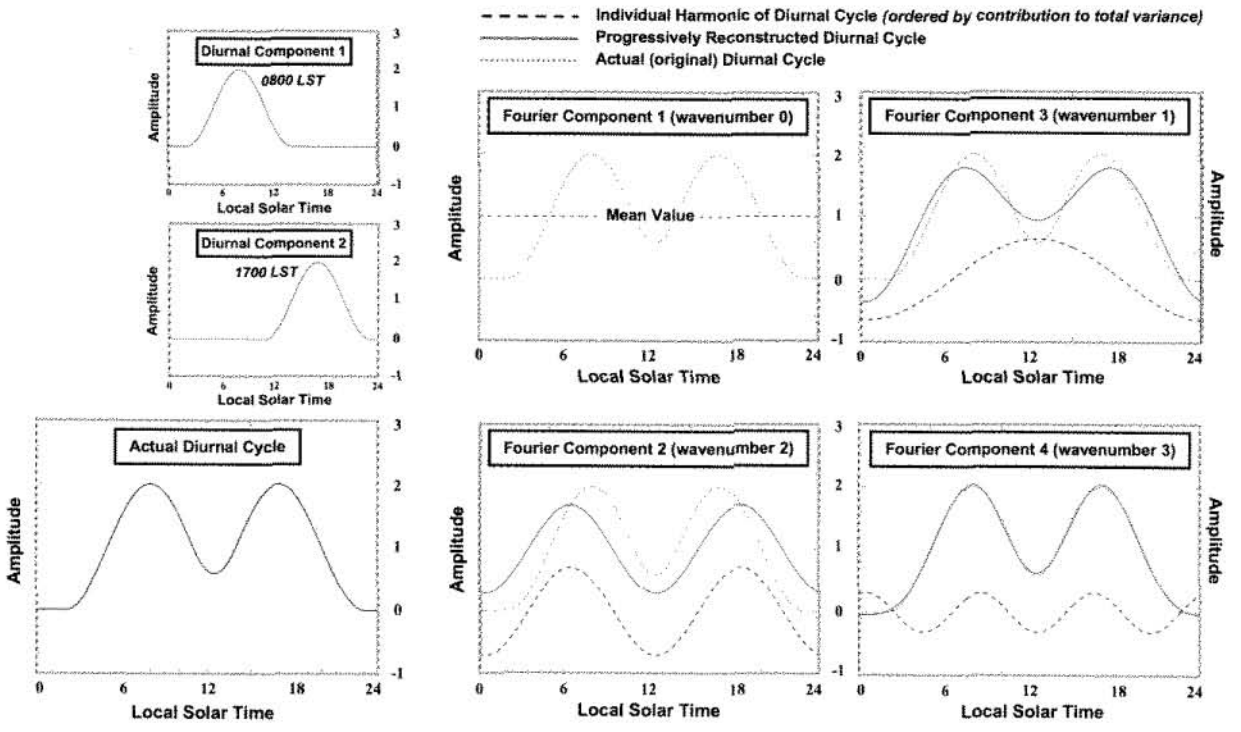

Figure 9: Fourier decomposition of two purely sinusoidal, but truncated, equal-amplitude and phase-shifted diurnal modes combined into two-peak diurnal cycle. Three left-hand panels show two separate diurnal modes along with combined diurnal cycle. Four right-hand panels show successive reconstructions of combined diurnal cycle using mean value (wave number 0) and first three principal Fourier harmonics (wave numbers 1 - 3).

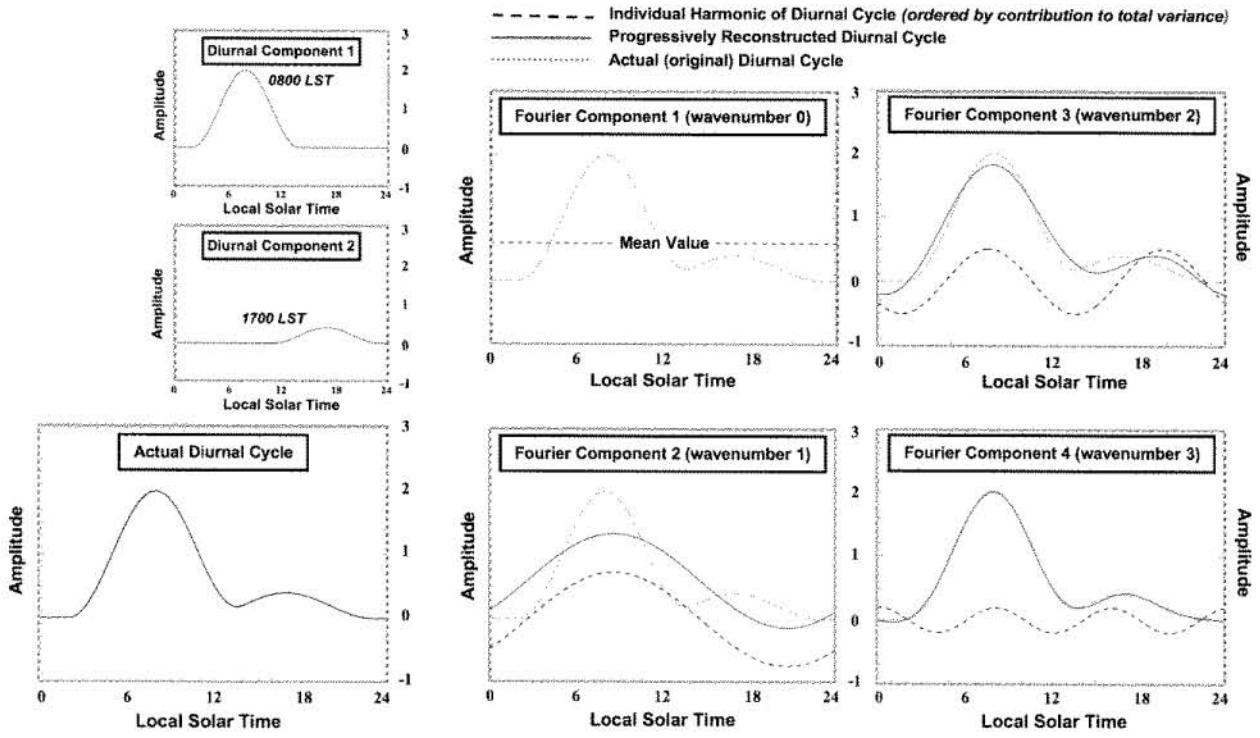

Figure 10: Same as in Fig. 9, except that two diurnal modes are unequal-amplitude.

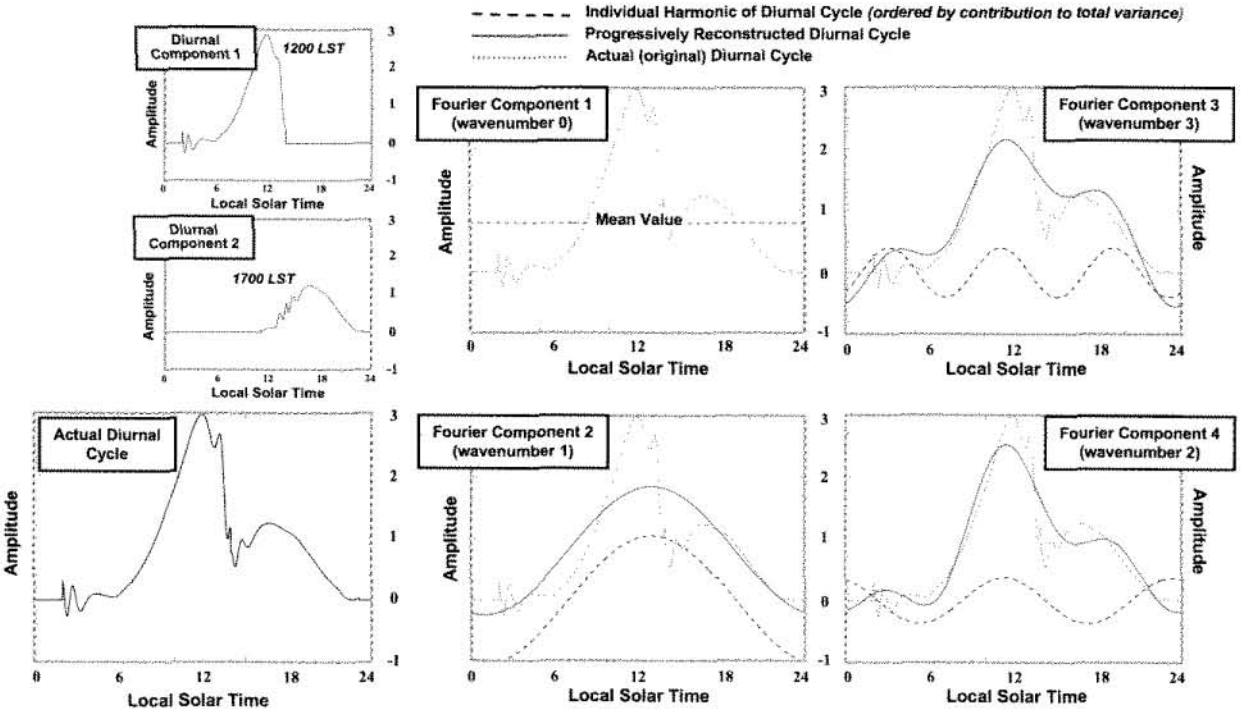

Figure 11: Same as in Fig. 9, except that two diurnal modes are realistic (non-sinusoidal and unequal-amplitude).